J Therm Anal Calorim (2014) 118:1721–1732
DOI 10.1007/s10973-014-4077-8

How to determine activation energy of glass transition

Roman Svoboda

Received: 3 January 2014 / Accepted: 3 August 2014 / Published online: 29 August 2014

Abstract The article critically reviews the current methodologies for determination of apparent activation energy of structural relaxation, Δh^*, in the glass transition range. Tool–Narayanaswamy–Moynihan phenomenological model was used to simulate data for all major types of relaxation behavior, which were consequently evaluated in terms of the tested methodologies (curve-fitting, evaluation of Δh^* from intrinsic cycles and evaluation of Δh^* from constant heating rate cycles). Advantages and disadvantages of particular methodologies are demonstrated and thoroughly discussed. In addition, effects of various data-distortive effects influencing determination of glass transition activation energy are demonstrated and described. The discussed data-distortive effects include presence thermal gradients, improperly designed temperature programs, incorrectly applied subtractions of the thermokinetic background, or inability of the DSC instrument to perform high cooling/heating rates. Detailed guide for correct determination of Δh^* from DSC measurements is introduced.

Keywords Glass transition · Activation energy · TNM model · Structural relaxation

Electronic supplementary material The online version of this article (doi:10.1007/s10973-014-4077-8) contains supplementary material, which is available to authorized users.

R. Svoboda (✉)
Department of Physical Chemistry, Faculty of Chemical Technology, University of Pardubice, Studentska 573, 532 10 Pardubice, Czech Republic
e-mail: roman.svoboda@atlas.cz; roman.svoboda@upce.cz

Introduction

Activation energy belongs to the most important quantities for each physical process, including the structural relaxation. [1] Its determination is often realized using the methods of thermal analysis (usually DSC or DTA)—it should be noted that in such case it is the macroscopic "apparent" activation energy that is being determined. In this regard, it is the nowadays trend to apply the simple Kissinger-type equations in order to determine the activation energy of glass transition. However, this wide-spread practice is in most cases incorrect because the Kissinger-type equations were derived for simple thermally activated processes and do not account for the complicated memory effects manifesting during the heating DSC scan over the glass transition region [2, 3].

Further confusion regarding the determination of apparent activation energy of glass transition/structural relaxation (Δh^*) arises from the fact that the most famous equations (associated with names as Moynihan, Hodge or Hutchinson) derived for proper determination of Δh^* are formally very similar to the Kissinger-type equations, with the only difference dwelling in the necessity for an appropriate temperature program being applied during the DSC measurement (the exact thermal history assures certain manifestation of the memory effects for the equations to be valid). This fact is very often overlooked by authors, who cite Moynihan, Hodge, or Hutchinson but apply their equations on data from simple heating scans of the as-prepared materials, which consequently leads to erroneous results.

It is the purpose of this article to review the correct methodologies for determination of the activation energy of glass transition/structural relaxation phenomenon, and discuss them with respect to the choice of appropriate experimental conditions and temperature programs.

Furthermore, detailed discussion over effects of all relevant experimental conditions and temperature programs variables will be conducted, so that even a non-expert may recognize data-distortions caused by these effects and adjust the experiment accordingly. In the end of the article, a detailed easy-to-apply guide for correct determination of glass transition activation energy will be introduced.

In the current article, we will employ the classical phenomenological Tool–Narayanaswamy–Moynihan model [4–6], which remains probably the most popular and widely used concept for description of structural relaxation behavior. This model is defined by the following equations:

$$\Phi(t) = \exp\left[-\left(\int_0^t \frac{\mathrm{d}t}{\tau(T, T_\mathrm{f})}\right)^{\beta}\right], \tag{1}$$

$$\tau(T, T_\mathrm{f}) = A \cdot \exp\left[x\frac{\Delta h^*}{RT} + (1-x)\frac{\Delta h^*}{RT_\mathrm{f}}\right], \tag{2}$$

where $\Phi(t)$ is the relaxation function of the given material property, t is time, τ is the relaxation time (depending both on temperature as well as on the actual structure of the material), β is the non-exponentiality parameter, A is the pre-exponential factor, x is the non-linearity parameter, Δh^* is the apparent activation energy of the structural relaxation, R is the universal gas constant, T is temperature, and T_f is the fictive temperature.

In the following texts, we will introduce appropriate methodologies for the determination of the apparent activation energy Δh^* for the TNM model: the determination from curve-fitting, determination from intrinsic cycles, and determination from constant heating rate cycles. Based on theoretically simulated data, a detailed discussion over the effects of various experimental conditions on accuracy of Δh^* determination will be conducted for the three methodologies.

Experimental

All theoretical simulations were based on the algorithm for the Tool–Narayanaswamy–Moynihan curve-fitting procedure, which can be found in [7]. Expressions for non-isothermal and isothermal steps are represented by the following equations, respectively:

$$T_{\mathrm{f,n}} = T_0 + \sum_{j=1}^{n} \Delta T_\mathrm{j}\left\{1 - \exp\left[-\left(\sum_{k=j}^{n} \Delta T_\mathrm{k}/q_\mathrm{k}\tau_\mathrm{k}\right)^{\beta}\right]\right\}, \tag{3}$$

$$T_{\mathrm{f,n}} = T_0 + \sum_{j=1}^{n_\mathrm{A}} \Delta T_\mathrm{j}\left\{1 - \exp\left[-\left(\sum_{k=n_\mathrm{A}}^{n} \Delta t_{\mathrm{e,k}}/\tau_\mathrm{k}\right)^{\beta}\right]\right\}, \tag{4}$$

where T_0 is the initial equilibrium temperature and t_e is the annealing time. The fictive temperature is then used to calculate the normalized heat capacity C_p^N; the output data are introduced as provided, i.e., in the C_p^N format:

$$C_\mathrm{p}^\mathrm{N} = \frac{\mathrm{d}T_\mathrm{f}}{\mathrm{d}T} = \frac{C_\mathrm{p} - C_\mathrm{pg}}{C_\mathrm{pl} - C_\mathrm{pg}}. \tag{5}$$

With regard to applied temperature programs, two types of thermal histories are usually applied to evaluate the apparent activation energy Δh^*. Both these thermal histories are based on cyclic experiments, i.e., the samples are alternately cooled and heated through the glass transition region at various cooling and heating rates. Both types of cyclic experiments are schematically visualized in Fig. 1. The two upper graphs (denoted "A") correspond to the constant heating rate (CHR) cycles, where cooling rates vary while the heating rates remain constant. Such temperature profile is depicted in the upper left graph. The upper right graph then shows typical normalized heat capacity response during the heating scan—the largest and most pronounced peaks correspond to cycles with slowest cooling. The second type of cyclic experiments, the so-called intrinsic cycles are displayed in the two lower graphs in Fig. 1 (denoted "B"). In these cycles, it is the ratio between the cooling and following heating rates q^+/q^-, which remains the same. The ratio is usually set equal to unity, i.e., the heating scans are performed at the same rate as was that of the previous cooling step. This temperature program is displayed in the lower left graph; the corresponding normalized heat capacity response obtained during the heating scans is depicted in the lower right figure.

In order to cover all types of structural relaxation behavior in our tests, various combinations of TNM parameters were used to simulate the DSC data ($C_\mathrm{p}^\mathrm{N} - T$ dependences). Three basic datasets were created for the following combinations of apparent activation energy and pre-exponential factor: 1. $\Delta h^*/R = 45$ kK and $\ln(A/\mathrm{s}) = 85$; 2. $\Delta h^*/R = 65$ kK and $\ln(A/\mathrm{s}) = 125$; 3. $\Delta h^*/R = 25$ kK and $\ln(A/\mathrm{s}) = 44.5$. The values of apparent activation energy were chosen to cover the most often observed Δh^* range for glassy and polymeric materials. The corresponding values of pre-exponential factor A were calculated for the glass transition effect to occur in a roughly similar temperature range in case of all three datasets. Each dataset further contains data for various combinations of the β and x parameters—for both parameters, the following discrete values were tested: 0.3, 0.6, and 0.9 (altogether giving 9 β/x combinations within each of the three basic datasets). These combinations again cover the most commonly observed types of non-exponentiality and non-linearity behaviors (both the parameters β and x may range from 0 to 1).

For each combination of the four TNM parameters, two sets of DSC curves were simulated, one set imitating an ideal measurement of intrinsic cycles and the second set

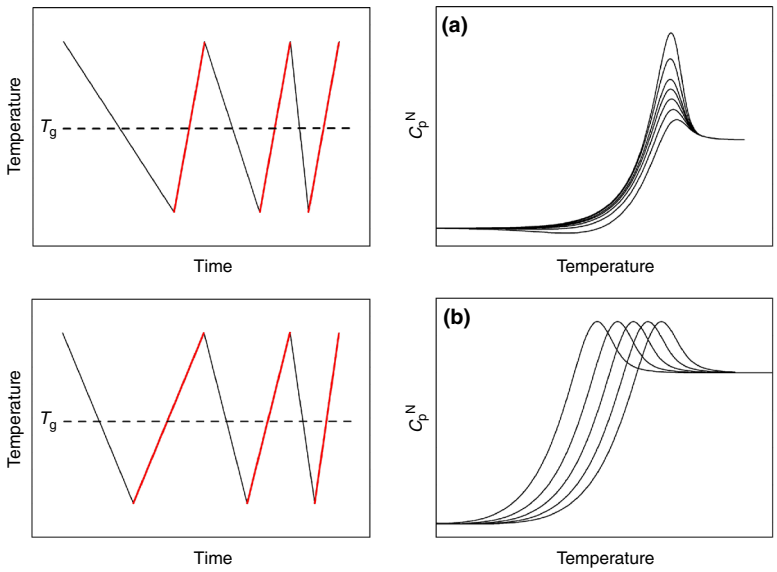

Fig. 1 Schematic representation of the three most common temperature histories (*left column*) used for studying relaxation behavior of amorphous materials. Usual DSC response during the measuring heating scans is displayed in the right column. Rows A and B correspond to the constant heating rate cycles and intrinsic cycles, respectively

imitating ideal measurements of CHR cycles. Regarding the specific temperature programs applied for these three basic datasets, the lower and upper temperature limits for cycles were set to 0 and 350 °C, respectively. Only in case of the third basic dataset ($\Delta h^*/R = 25$ kK and $\ln(A/s) = 44.5$), these limits were for the CHR cycles extended to -50 and 400 °C. The heating rates were set as follows : in case of intrinsic cycles, the similar cooling and consequent heating rates were used ($q^+/q^- = 1$), the specific values were 0.5, 1, 2, 5, 10, 20, and 50 C min^{-1}; in case of CHR cycles, the simulated cooling rates were 0.5, 1, 2, 5, 10, 20, and 50 C min^{-1}, while the heating rate was set constant $q^+ = 10$ °C min^{-1}. Each cycle, i.e., the cooling and the consequent heating step, was simulated separately to ensure the equilibrated initial state and erased thermal history.

For better understanding, the first basic dataset of CHR cycles is depicted in Fig. 2. All the curves in Fig. 2 were simulated for $\Delta h^*/R = 45$ kK and $\ln(A/s) = 85$ (the "first" basic dataset); the used values of β and x parameters are suggested in figure—non-exponentiality differs with rows while the non-linearity differs with columns. Each graph then shows heating scans (all performed at 10 °C min^{-1}) following different cooling steps, where the most pronounced relaxation peaks correspond to response to cooling at 0.5 °C min^{-1} and the least pronounced relaxation peaks correspond to the response to cooling at 50 °C min^{-1}. The cooling steps are not displayed as they are not used for the evaluations. All six basic datasets (three for the intrinsic cycles and three for the CHR cycles) can be found in ESM of Appendix 1. These basic datasets correspond to ideally performed DSC experiments and will serve as a reference for the further studies of various data-distortive effects.

Results and discussion

In the Results and discussion, three most important methodologies for calculation of the apparent activation energy of structural relaxation will be discussed; accent will be put on influence of various experimental conditions on correctness and accuracy of the determined Δh^* value.

Curve-fitting procedure

In curve-fitting, the parameters of the TNM model are obtained via non-linear optimization methods. The optimization may be realized e.g., by the Levenberg–Marquardt algorithm and searching for the minimum of the residual sum of squares (RSS) in order to obtain the best fit. The curve-fitting provides a very precise way of TNM parameters determination. However, as such it is also the most susceptible method to erroneous results caused either by incorrect optimization procedure or by data-distortive effects.

Regarding the correctness of the non-linear optimization, it has to be borne in mind that there is high correlation between the four TNM parameters, which leads to high number of local RSS minima. Consequently, the optimization procedure needs to be tested for various combinations of initial input parameter values so that the acquirement of the absolute RSS minimum is confirmed. Reduction of variable parameters is usually not an option in this case because there are simply no sufficiently precise alternative methods for their determination.

Theoretically, the curve-fitting procedure is applicable to data for any temperature history, no matter how complicated it is. However, the more the temperature history is complicated the higher is the potential for data-distortive

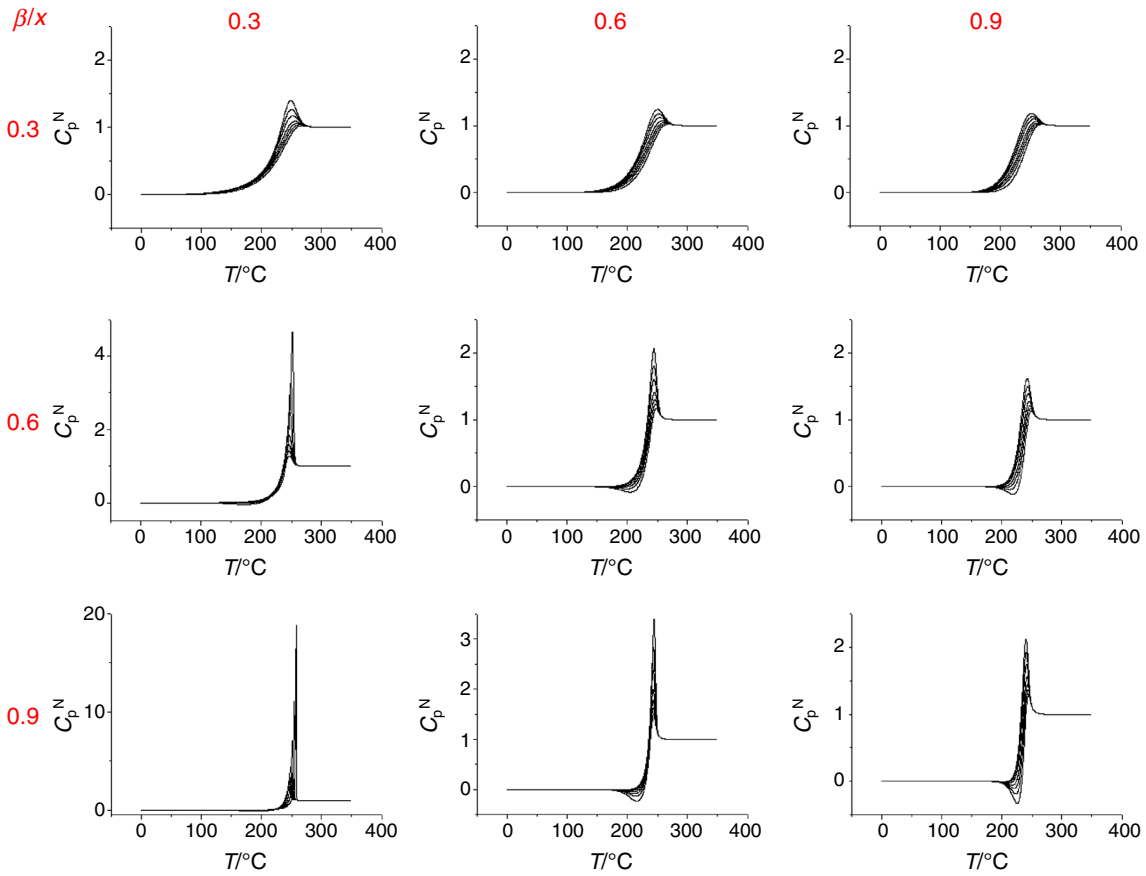

Fig. 2 Simulated datasets corresponding to thermal history of constant heating rate cycles for various combinations of certain TNM parameters. Input parameters were $\Delta h^*/R = 45$ kK, $\ln(A/\mathrm{s}) = -85$, values of x and β differ in case of each graph and are suggested in the figure (columns differ in x, rows differ in β)

effects to occur and manifest. In this regard, the following plays most important role: stability of the sample, stability of experimental conditions during long temperature programs (isotherms), stability and accuracy of applied heating and cooling rates, initial delays before the constant rate is achieved after an isothermal step or the thermal lag effects at instant heating → cooling and cooling → heating transitions. For this reason, it is customary to perform curve-fitting on data with simple thermal history—such as the cyclic experiments. In addition to the simplicity and rather short duration of the experiment, it is also important for all structural relaxation features to manifest significantly so that the mutual correlations between the TNM parameters equally contribute during the optimization procedure. In this respect, the CHR cycles are optimal (contrary to the intrinsic cycles where the degree of nonlinearity remains similar for all the cycles).

Apart from the data-distortive effects originating from unideal correspondence between the programed and truly realized temperature histories, the data can be also distorted during their preparation for the curve-fitting procedure. In this regard, it is namely the subtraction of the thermokinetic background (baseline, zeroline …), which plays a crucial role. Example of such distortion was shown in our previous work [8]: to demonstrate the danger of mistreating the relaxation data, we have tested the influence of an incorrect thermokinetic background subtraction. For this reason, two sets of relaxation DSC curves were prepared—set A corresponding to the true DSC signal of the CHR cycles, and set B corresponding to the data with an incorrectly subtracted zeroline, where undershoot was ignored. Both these datasets are displayed in Fig. 3 (reproduced from [8], where the details about temperature history can be found), for clarity, the incorrect data are shifted in temperature by 50 °C. As can be seen, there are subtle but significant differences in the data; however, without further supplemental information there would be no way of distinguishing (by their appearance) the correct and incorrect datasets. This relatively subtle distortion of the data, however, leads to a huge difference in evaluated TNM parameters (for Δh^* the error was higher than 40 % ~180 kJ mol^{-1} in that

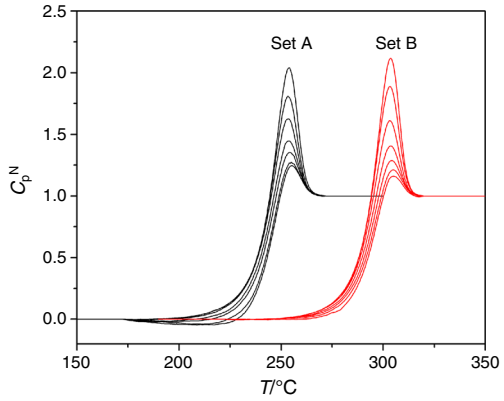

Fig. 3 Relaxation response of $Ge_2Sb_2Se_{4.5}Te_{0.5}$ glass obtained during constant heating rate cycles [8]. Dataset A corresponds to correctly treated and normalized data; dataset B then represents data where zeroline was incorrectly subtracted (the data were shifted to higher temperature—about 50 °C—for better clarity). Figure is reproduced from [8]

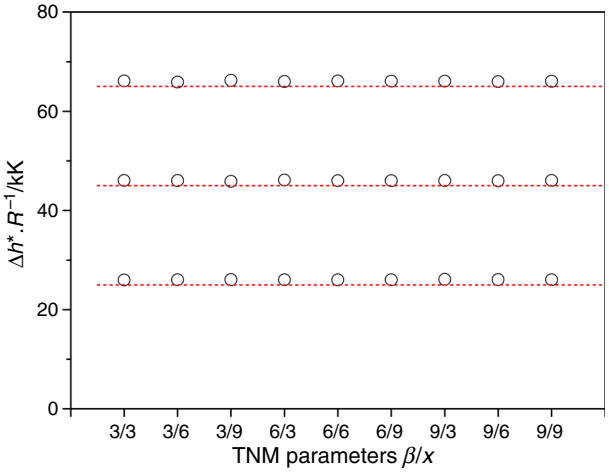

Fig. 4 Evaluation of $\Delta h^*/R$ from intrinsic cycles for all simulated datasets. The theoretical input $\Delta h^*/R$ values (25, 45 and 65 kK) are suggested by *dashed lines*. The tested combinations of β and x parameters are given in the β/x format on the X axis (e.g., 6/3 corresponds to data simulated for $\beta = 0.6$ and $x = 0.3$)

particular case [8]). Though, proper recognition of the subtle undershoot effects is often very difficult due to the non-linear $C_p - T$ dependencies and may require certain experience on the part of the researcher. In case of doubt, the general rule of thumb is to check the consistency of evaluated TNM parameters with respect to the changing experimental conditions (e.g., cooling rate in case of the CHR cycles)—all the evaluated parameters should be independent of the experimental conditions. [8] This is also why the curve-fitting should be always applied to several data-curves with significantly different temperature histories. In this regard, a great care has to be taken especially in case of simultaneous fitting of multiple data-curves, when the averaged values of the relaxation parameters may conceal a hidden dependence on experimental conditions.

Evaluation from intrinsic cycles

Intrinsic cycles (see Fig. 1b) can be used for the evaluation of apparent activation energy of structural relaxation according to the following equation:

$$-\frac{\Delta h^*}{R} = \left[\frac{\mathrm{d}\ln|q^+|}{\mathrm{d}\left(1/T_\mathrm{p}\right)}\right]_{q^-/q^+=\mathrm{const}}, \qquad (6)$$

where T_p stands for the temperature corresponding to the maximum of the relaxation peak (overshoot). This equation is based on the peak-shift method [9, 10], and it can be directly deduced from article by Hutchinson and Ruddy [11]. Nevertheless, to our knowledge, Eq. 6 was never actually derived and expressed in the above-shown form by the original authors, nor it was tested on theoretically simulated data. Therefore, we have at first subjected the equation to extensive testing—the three basic datasets theoretically simulated for the intrinsic cycles' temperature history (see ESM of Appendix 1 and "Experimental part" section) were utilized in this regard. For each set of theoretical curves corresponding to a given combination of the four TNM parameters, the Δh^* value was determined using Eq. 6. In Fig. 4, the determined values of reduced apparent activation energy are displayed for all three datasets in comparison with the true $\Delta h^*/R$ values input into the simulation procedure (25, 45, and 65 kK, suggested by dashed lines) in dependence on the respective combinations of β and x TNM parameters (where e.g., 6/3 corresponds to $\beta = 0.6$ and $x = 0.3$). As can be seen, the agreement is very good for all combinations of relaxation parameters, though a slight systematic shift can be observed. The average $\Delta h^*/R$ values obtained for the three evaluated datasets were 26.03 ± 0.03, 46.00 ± 0.06, and 66.04 ± 0.09 kK, respectively. Thus, it can be summarized that the systematic error associated with the Δh^* determination according to Eq. 6 (taking into account reasonable and physically meaningful values of activation energy) varies between 1 and 4 %, with the highest errors being recorded for lowest apparent activation energies. Origin of this systematic error lies in a simplifying presumption that was taken during the derivation of Eq. 6, namely that T_g and T_p behave similarly with respect to the heating rate. In conclusion, the determination of apparent activation energy of structural relaxation according to Eq. 6 provides very reasonable results burdened by only very small and constant systematic error (equal to approximately +1 kK).

Apart from the fundamental testing of Eq. 6 (described in the previous paragraph), effects of various experimental conditions and their influence on accuracy of Δh^* determination according to Eq. 6 were examined. We would like to state beforehand that qualitatively similar conclusions were obtained for all three basic datasets (i.e., for all three values of $\Delta h^*/R$ input in simulations—25, 45, and 65 kK). Therefore, from now on only the data for the first basic dataset ($\Delta h^*/R = 45$ kK and $\ln(A/\mathrm{s}) = 85$) will be used to demonstrate the influences of the respective studied experimental conditions.

Choice of temperature range

First, the choice of proper temperature range for the intrinsic cycle measurements was tested. It is believed that during the cyclic measurements, the true undercooled liquid and glassy states should always be reached to obtain correct data and results. It may, however, be sometimes problem to determine whether the true glassy state was already reached. In addition, it is also advantageous not to set the temperature range for cyclic experiments too wide in order to shorten the measurement and reduce the baseline drift due to long-term instability of the instrument. In this regard, three new datasets were simulated in order to imitate various effects of improper (too narrow) temperature range choice. In the first dataset, the lower and upper temperature limits for intrinsic cyclic experiments were set to be 180 and 350 °C, respectively. In the second dataset, the limits were 150 and 350 °C, and in the third dataset, the limits were 120 and 350 °C but in this last case there was an additional 1 h long isothermal segment inserted in-between the cooling and consequent heating steps (the latter imitates a possibility of occurrence of a certain delay during the instant change from cooling to heating; the chosen 1 h duration represents a multifold extreme, unreachable under real conditions, where similar delays last several tenths of seconds most). All three complete datasets can be found in ESM of Appendix 2.

It was found that for most β/x combinations, it is critical to cool the undercooled liquid "only" through the temperature range in which the major structural change occurs. Once the temperature decreases below the extrapolated glass transition to $C_p^N \approx 0.25$ (or lower), the incomplete transformation into the glassy state does not significantly influence the reverse transformation toward the undercooled liquid state (applied within each cycle) because during heating the structural differences are erased and the temperature-dependent component of the relaxation process reinstates the course of transformation before T_p is reached. Incomplete achieving of the true glassy state has the strongest influence on materials with low value on nonlinearity parameter (weak dependence of relaxation on

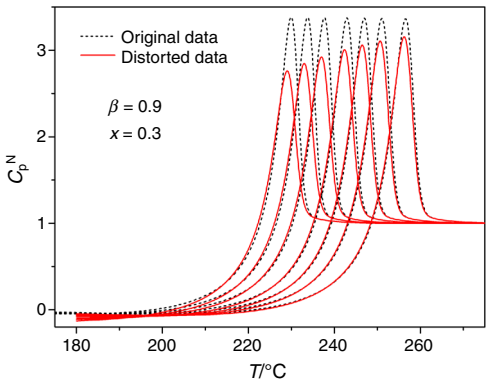

Fig. 5 Distortion of a set of intrinsic cycles heating scans simulated for $\Delta h^*/R = 45$ kK, $\ln(A/\mathrm{s}) = -85$, $\beta = 0.9$, and $x = 0.3$. *Dashed lines* correspond to the original undistorted data, while the *solid lines* correspond to the distorted data where the cooling steps were performed only down to 180 °C (true glassy state was not yet reached during these steps)

temperature and strong dependence on actual structure). Such materials show characteristic distortion of the heating scan data during intrinsic cycles. Example of such behavior is shown in Fig. 5, where the undistorted data (for $\beta = 0.9$ and $x = 0.3$) from the original dataset No. 1 (dashed lines) are compared to the corresponding set of curves simulated for cooling only down to 180 °C. In Fig. 5, it can be seen that incomplete reaching of the true glassy state may in special cases (highly non-linear along with weakly non-exponential relaxation behavior) cause decrease of the relaxation overshoot and its slight shift to lower temperature. Naturally, this distortion occurs in dependence on degree of incompletion of reaching the glassy state, i.e., the slower the cooling, the larger is the deformation.

Complete results on the first set of tests are displayed in Fig. 6, where the difference in reduced apparent activation energy of structural relaxation (calculated as $\Delta h^*/R$ calculated from distorted data minus $\Delta h^*/R$ calculated from the original undistorted data) is shown for all studied β/x combinations. Except for the specific combination of relaxation features mentioned in the previous paragraph (highly non-linear along with weakly non-exponential relaxation behavior), the error in $\Delta h^*/R$ caused by incomplete achieving of the true glassy state during intrinsic cycles is negligible (under 0.5 %) but even in the case of $\beta/x = 9/3$, the error was only ~ 2 %. Similar finding was obtained also in case of shorter (up to 1 h) isothermal relaxation segments inserted in-between the cooling and consequent heating steps (full points in Fig. 6).

Choice of heating and cooling rates

Second set of tests performed for the intrinsic cycles concerns the choice of heating rates. The basic condition for

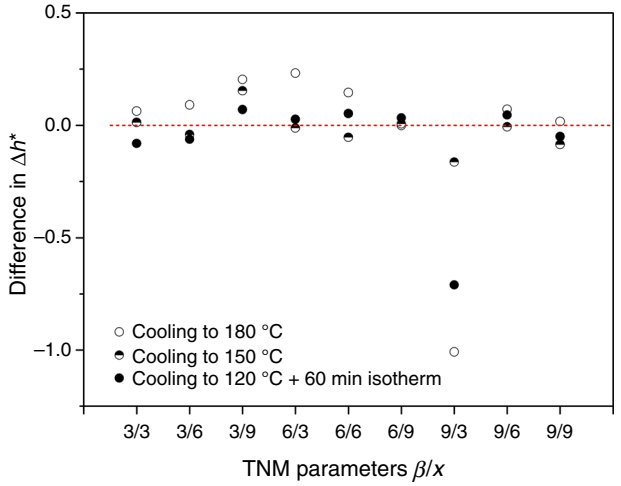

Fig. 6 Calculated differences in reduced apparent activation energy ($\Delta h^*/R$ distorted minus $\Delta h^*/R$ undistorted) for various data-distortive effects applied in case of intrinsic cycles. All the simulations were performed for $\Delta h^*/R = 45$ kK, $\ln(A/s) = -85$; the particular combinations of β and x parameters are given on the X axis. The distortions were caused by performing the cooling steps only down to the suggested temperatures: 180, 150, and 120 °C; in case of the latter a 60 min isotherm was inserted in-between the cooling and heating steps

applicability of Eq. 6 is the constancy of ratio between the cooling and consequent heating rates ($q^+/q^- = \text{const.}$). Common practice is to apply heating rate of the same magnitude as was that of the previous cooling ($q^+/q^- = 1$). Nevertheless, in principle it is possible to choose any q^+/q^- ratio. In particular, the q^+/q^- ratios ~ 2 are of significant interest due to several reasons: broader range of cooling and heating rates can be applied—it is much easier to realize slower cooling rates as the fast cooling is often limited only to a certain temperature region and cannot be performed down to ambient temperatures; also, the higher cooling rates result in better, more pronounced signal, which improves the evaluation options for the heating scans following cooling steps performed at very slow cooling rates. Both these factors would be further improved for $q^+/q^- > 2$ ratios but in such case, serious thermal lags distorting the DSC signal during the very fast heating rates might occur. Therefore, for most DSCs, the $q^+/q^- = 2$ ratio is probably optimal. To test the above-mentioned option, we have simulated three datasets with $q^+/q^- = 2$ (otherwise analogous to the three basic datasets Nos. 1–3) and evaluated the apparent activation energy for all the combinations of TNM parameters. The resulting $\Delta h^*/R$ values were similar as in case of the basic datasets (the differences were approx. ±0.1 kK, which corresponds to the error of evaluation). Hence, from the theoretical methodology point of view, the choice of q^+/q^- has no effect on its outcome.

Furthermore, we have also tested influence of the main data-distortive effects related to heating rates and occurring during intrinsic cycles. First, we have simulated a situation when the fastest heating rates would be too high for the instrument to perform; such situation is likely to arise for higher q^+/q^- ratios. Such a case is demonstrated in Fig. 7a, where the set of simulated curves for $\Delta h^*/R = 45$ kK, $\ln(A/s) = 85$, $\beta = 0.6$, and $x = 0.6$ is shown for the $q^+/q^- = 2$ intrinsic cycles temperature history. The "original" and "undistorted" data correspond to the ideal situation, when the heating rates actually realized in the DSC instrument match the programed thermal history. The "distorted" data, on the other hand, correspond to the situation, when in case of the high heating rates the DSC instrument is not capable to perform the programed heating rate—to imitate this behavior the heating rate $q^+ = 40$ °C min^{-1} was for the purpose of simulation lowered by 10 % (to 36 °C min^{-1}) and the heating rate $q^+ = 100$ °C min^{-1} was lowered by 20 % (to 80 °C min^{-1}). In Fig. 7a, the left graph shows the actual simulated curves, while the right graph depicts the evaluation according to Eq. 6.

Another data-distortive effect can be associated with limited cooling capabilities of certain DSCs, i.e., in case of high programed cooling rates, the DSC instrument would not be able to perform them and the actually realized cooling rate would be lower than the programed one. Similar simulation as in the previously mentioned case was performed to demonstrate effect of such data-distortion—set of simulated intrinsic cycles curves for $\Delta h^*/R = 45$ kK, $\ln(A/s) = 85$, $\beta = 0.6$, $x = 0.6$, and $q^+/q^- = 1$ was used as a base dataset. To imitate the distortion, the cooling rate $q^+ = 20$ °C min^{-1} was for the purpose of simulation lowered by 10 % (to 18 °C min^{-1}) and the cooling rate $q^+ = 50$ °C min^{-1} was lowered by 20 % (to 40 °C min^{-1}). In Fig. 7b, the corresponding simulated DSC curves (left graph) and the consequent evaluation according to Eq. 6 (right graph) are shown. In a concurring test, we have simulated a more common situation where the difference between the programed and truly achieved cooling rates arises only when certain (low enough) temperature is reached. If this deviation from the programed cooling rate occurs after the true glass state is reached (or almost reached), the change of the cooling rate has no effect on the consequent heating scan, and thus the Δh^* remains the same.

As can be seen in Fig. 7, both the above-mentioned data-distortive effects result in a similar shift of T_p toward lower temperatures (occurring at higher q^+), leading to higher values of apparent activation energy Δh^*. The true nature of the respective data-distortive effects can then be identified based on the difference in their manifestation during the DSC measurements—as shown in Fig. 7, the effective decrease of

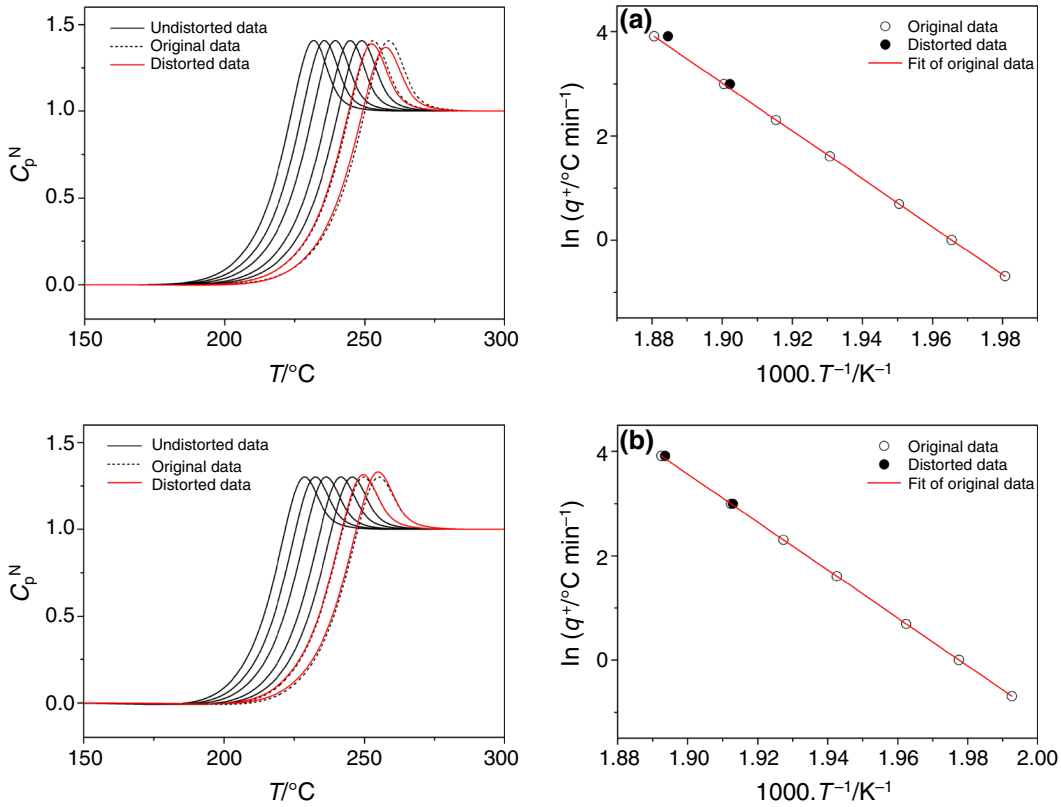

Fig. 7 Demonstration of two types of data-distortive effects occurring for intrinsic cycles. All the data were simulated for $\Delta h^*/R = 45$ kK, $\ln(A/s) = -85$, $\beta = 0.6$, and $x = 0.6$. Row A corresponds to $q^+/q^- = 2$; the distortion imitates inability of DSC instrument to perform very high heating rates. Row B corresponds to $q^+/q^- = 1$; the distortion imitates inability of DSC instrument to perform very high cooling rates. Left column compares the distorted and undistorted DSC curves, while the right column projects this distortion into the evaluation of Δh^*

heating rates results in decrease of the DSC overshoot (upper left graph), while the effective decrease of cooling rates results in increase of the DSC overshoot (lower left graph).

Lastly, we have also tested the data-distortive effect associated with thermal lags occurring in the sample. Majority of DSCs are calibrated on melting temperatures of pure metals. In such case, an ideal thermal contact is usually established in-between the DSC pan bottom and thin layer of pre-molten metal. Nevertheless, in case of real samples (bulks, powders etc.), some sort of thermal lag often arises due to the unideal contact of the sample with the pan bottom. To imitate this effect, we have taken the intrinsic cycles data simulated for $\Delta h^*/R = 45$ kK, $\ln(A/s) = 85$, $\beta = 0.6$, $x = 0.6$, and $q^+/q^- = 1$ as base undistorted dataset and assumed that it takes 3 extra seconds for the real sample to adopt the temperature of the furnace/pan and for the response signal to reach the sensor. Such thermal lag results in temperature shift of the maximum of the relaxation peak ΔT_p, varying with the applied heating rate (e.g., for 20 °C min^{-1} the 3 s thermal lag would result in $\Delta T_p = 1$ °C). The above-described data-distortive effect is demonstrated in Fig. 8; it can be seen that the distortion manifests as a curvature at higher heating rates, resulting in lower values of apparent activation energy Δh^*. This is also the main way how to recognize this type of data-distortion, as the raw DSC data normalized to C_p^N show only a slight shift toward higher temperatures, while the overall shape of the curve (including the relaxation peak height) remains the same.

Evaluation from CHR cycles

Apparent activation energy of structural relaxation can be evaluated from CHR cycles according to the following equation [6, 12]:

$$-\frac{\Delta h^*}{R} = \frac{d\ln|q^-|}{d\left(1/T_f\right)}, \tag{7}$$

where the fictive temperature T_f corresponds to the conventional T_g value obtained on cooling, i.e., to the temperature of intersection of the extrapolated liquid and glass property-T curves (that is why the evaluation is sometimes referred to as "determination of Δh^* from dependence of T_g on cooling"). The structure of the glass achieved during the cooling step (represented by T_f) can be evaluated using

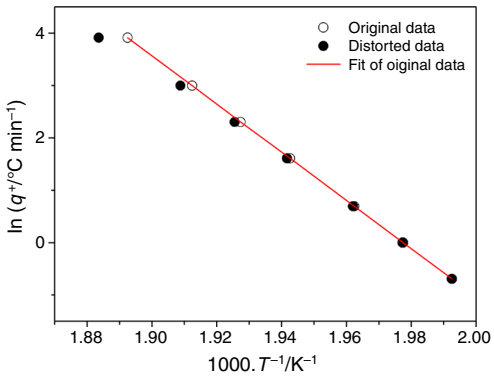

Fig. 8 Demonstration of data-distortive effect associated with thermal lag occurring during intrinsic cycles and its influence on Δh^* evaluation. Data correspond to the following set of TNM parameters: $\Delta h^*/R = 45$ kK, $\ln(A/\mathrm{s}) = -85$, $\beta = 0.6$, and $x = 0.6$; the $q^+/q^- = 1$ ratio and 3 s long thermal lag were applied

the "equal area method" [6, 12]. This method is based on the following equation:

$$\int_{T^*}^{T_\mathrm{f}} \left(C_\mathrm{pl} - C_\mathrm{pg}\right)\mathrm{d}T_\mathrm{f} = \int_{T^*}^{T'} \left(C_\mathrm{p} - C_\mathrm{pg}\right)\mathrm{d}T, \tag{8}$$

where T^* is any temperature above T_g at which the heat capacity is equal to the equilibrium undercooled liquid value C_pl and $T'$is a temperature well below T_g where a constant glassy value of C_pg was achieved.

The evaluation of Δh^* from CHR cycles is a well-established method; therefore, no extensive testing of the methodology itself was needed. Nevertheless, we have performed similar testing of the basic functioning of this method similarly as in case of Eq. 6. In Fig. 9, the resulting values of reduced apparent activation energy evaluated according to Eq. 7 for all three basic datasets are shown. As can be seen, again the obtained $\Delta h^*/R$ values are slightly higher than the true activation energies input into the simulation, though the difference is lower than in case of evaluation from intrinsic cycles. The average $\Delta h^*/R$ values obtained for the three evaluated datasets were 25.83 ± 0.14, 45.90 ± 0.10, and 65.93 ± 0.08 kK, respectively, which again corresponds to a very reasonable agreement and hence validates results provided by this methodology.

In the following texts, the data-distortive effects associated with (im)proper selection of temperature range for the experiment as well as the effects associated with heating rates will be tested with respect to their influence on the Δh^* evaluation according to Eq. 7. These effects will again be demonstrated only qualitatively for selected combinations of TNM parameters. General validity of the derived conclusions was, however, verified for all parameter combinations included in the three basic datasets (see "Experimental part" section).

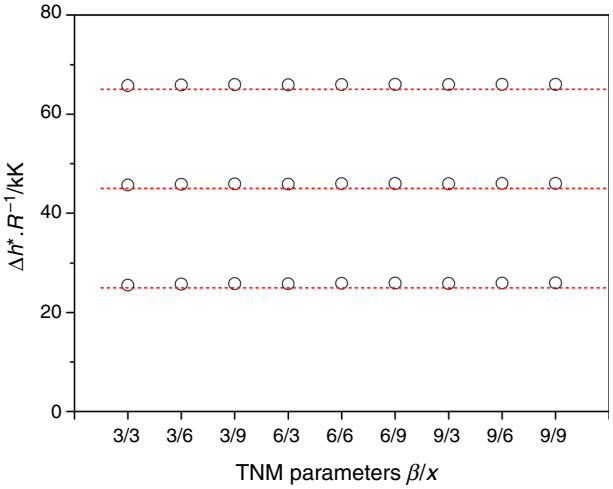

Fig. 9 Evaluation of $\Delta h^*/R$ from constant heating rate cycles for all simulated datasets. The theoretical input $\Delta h^*/R$ values (25, 45 and 65 kK) are suggested by *dashed lines*. The tested combinations of β and x parameters are given in the β/x format on the X axis (e.g., 6/3 corresponds to data simulated for $\beta = 0.6$ and $x = 0.3$)

Choice of temperature range

In order to test the influence of improper choice of temperature range for CHR experiments, where the material would not fully reach the true glassy state during the cooling step, two sets of curves were chosen as model examples. The first set of curves corresponds to the CHR data simulated for $\Delta h^*/R = 45$ kK, $\ln(A/\mathrm{s}) = 85$, $\beta = 0.3$, $x = 0.3$—these data represent a situation when no recognizable undershoot manifests during the heating scans. The second set of curves then corresponds to the CHR simulations performed for $\Delta h^*/R = 45$ kK, $\ln(A/\mathrm{s}) = 85$, $\beta = 0.6$, $x = 0.3$; the data represent relaxation behavior where undershoot can be observed during the measurements. In case of each set of curves, the influence of various low-temperature limits on Δh^* evaluation was tested.

The first set of undistorted CHR curves (corresponding to $\beta/x = 3/3$) is shown in Fig. 10a together with the tested low-temperature limits down to which the particular simulations were performed (dashed lines). The inset then shows the $\Delta h^*/R$ values determined according to Eq. 7 for the respective sets of curves simulated for the chosen low-temperature limits (the reduced activation energies are plotted in dependence on the T values used as low-temperature limits in the respective simulations). Similar graphs are for the $\beta/x = 6/3$ combination of TNM parameters shown in Fig. 10b—the first point shown in the inset (at $T = 0$ °C) again corresponds to undistorted $\Delta h^*/R$ value determined from the original basic dataset. As can be seen, in case of the first tested β/x combination (Fig. 10a), it is only the significant cutaway experiments,

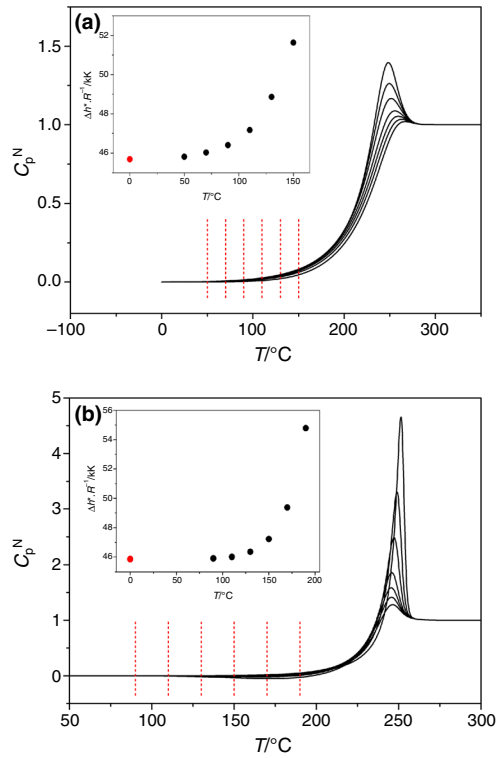

Fig. 10 Demonstration of data-distortive effects associated with improper choice of temperature range occurring during constant heating rate cycles. Graph A corresponds to data for $\Delta h^*/R = 45$ kK, $\ln(A/s) = -85$, $\beta = 0.3$, $x = 0.3$, and $q^+ = 10$ °C min^{-1}; in graph B then $\beta = 0.6$. *Dashed lines* suggest low-temperature limits down to which for each of them a simulation of a set of CHR curves was performed. The insets then show the $\Delta h^*/R$ values determined for the respective sets of curves (values on X axes correspond to the respective low-temperature limits)

which lead to markedly deviated $\Delta h^*/R$ values. However, such improper choice of the temperature interval for CHR cycles is improbable for relaxation behavior where no undershoots manifest. On the other hand, in case of the second set of curves (Fig. 10b) significantly distorted $\Delta h^*/R$ values are obtained even when the low-temperature limits are set only to the middle of the undershoot effect. As the undershoot effects may often be indistinctive and hence easily unrecognized (especially when $C_p - T$ dependence is non-linear in the vicinity of T_g), the situation displayed in Fig. 10b demonstrates an ever-present danger. To prevent unrecognition of an undershoot, CHR cycles including high cooling rates should be always applied during the pre-experimental testing (if only to properly set the temperature range); also, an increased value of the CHR prohibits manifestation of undershoots and the situation may therefore effectively transform into that displayed in Fig. 10a.

Contrary to the intrinsic cycles, distortions of either raw or normalized DSC data cannot be easily recognized in case of the CHR cycles. Therefore, most distortions have to be identified by means of the $\ln(q^-) - 1/T$ dependencies. In Fig. 11, the two main types of data-distortive effects associated with improper temperature range selection are demonstrated for the $\Delta h^*/R = 45$ kK, $\ln(A/s) = 85$, $\beta = 0.6$, $x = 0.3$ set of CHR curves (original data are depicted in Fig. 10b). Full symbols display distortion caused by setting the low-temperature limit too high, so that the true glassy state is not reached during cooling. In such case it is the data for lowest cooling rates, which are deviated most (toward higher fictive temperatures), although the linearity of the dependencies remains fair. This generally results in higher $\Delta h^*/R$ values. Second type of data-distortion, demonstrated by half-full symbols, corresponds to the situation when isothermal segment was inserted in-between the cooling and heating steps. In this particular case, we have applied an extremely long isotherm in order for the distortion to be better pronounced—the reasoning is similar to that introduced for the similar situation in case of intrinsic cycles (see "Choice of temperature range" section—full symbols in Fig. 6 and the corresponding discussion). As apparent, insertion of an isothermal segment, where the glass is allowed to relax, results in a characteristic positive curvature manifesting at high cooling rates. Regardless from the evaluated range of cooling rates used within the CHR cycles, this type of distortion again always results in higher $\Delta h^*/R$ values.

Choice of heating and cooling rates

The concept of CHR cycles relies on utilization of various cooling rates while using a CHR. Contrary to the intrinsic cycles, in case of the CHR cycles, the choice of heating rate may be crucial. The standard, most often utilized option is $q^+ = 10$ °C min^{-1}. However, by utilization of higher heating rates (20 or 30 °C min^{-1}) certain advantages can be gained. Most importantly, by application of higher heating rate the overall DSC signal increases, providing better sensitivity, and thus suppressing the influence of various data-distortive effects (inaccurate determination of $C_{pg} - T$ and $C_{pl} - T$ dependencies, improper zeroline subtraction etc.). In addition, at higher heating rates the undershoot effects cease to manifest, which effectively nullifies the main source of errors associated with Δh^* evaluation from CHR cycles (discussion about the errors associated with CHR cycles can be found in "Curve-fitting procedure" section, see also Fig. 3). Advantages of utilization of higher q^+ are well demonstrated in Fig. 12, where two sets of CHR curves simulated for $\Delta h^*/R = 45$ kK, $\ln(A/s) = 85$, $\beta = 0.6$, $x = 0.6$ are compared (one set was simulated for $q^+ = 10$ °C min^{-1}, while the other was simulated for $q^+ = 30$ °C min^{-1}). The set of curves simulated for $q^+ = 30$ °C min^{-1} was shifted by 50 °C to improve clarity. As can be seen, the curves simulated for

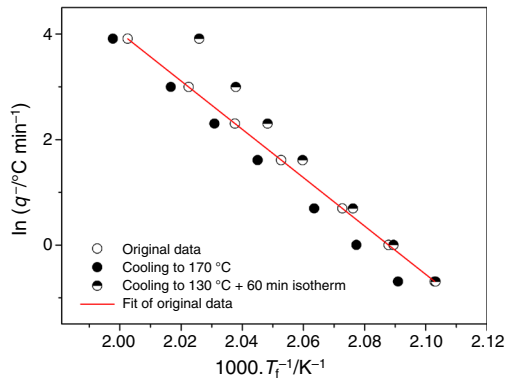

Fig. 11 Demonstration of data-distortive effects associated with improper choice of temperature range occurring during constant heating rate cycles. The data were simulated for $\Delta h^*/R = 45$ kK, $\ln(A/s) = -85$, $\beta = 0.6$, $x = 0.3$, and $q^+ = 10$ °C min^{-1}. The distortions were caused by performing the cooling steps only down to the suggested temperatures: 170 and 130 °C; in case of the latter a 60 min isotherm was inserted in-between the cooling and heating steps

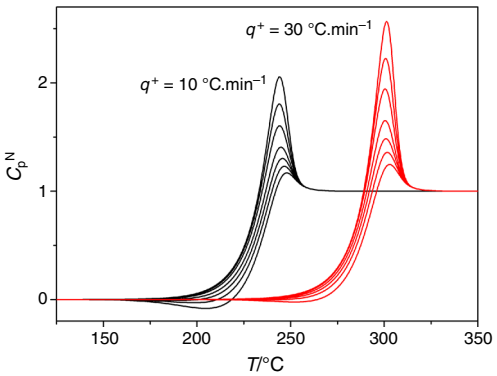

Fig. 12 Influence of a choice of heating rate for the constant heating rate cycles—the data were simulated for $\Delta h^*/R = 45$ kK, $\ln(A/s) = -85$, $\beta = 0.6$, and $x = 0.6$. Set of curves simulated for $q^+ = 30$ °C min^{-1} was shifted by 50 °C to improve clarity of the figure

higher heating rate are significantly more pronounced, and undershoot effects are greatly suppressed. The determined value of apparent activation energy was exactly the same for both sets of CHR curves—similar resemblance was found for all tested combinations of TNM parameters.

Furthermore, influences of data-distortive effects similar to those discussed in "Choice of heating and cooling rates" section were examined. Contrary to the intrinsic cycles, in case of CHR cycles only a single heating rate is used for whole set of measurements, which is why its magnitude does not really matter with regard to the Δh^* evaluation. Even in case when very fast heating rate was programed into the DSC the instrument could not match the required temperature increase, the deceleration would be similar for all heating scans (because similar high q^+ would have been originally programed for all cycles) and the effective result would correspond to a situation when lower (maximum truly available) CHR was programed for the measurements.

Different situation arises in case of data-distortions based on mismatching cooling rates. To imitate the limited cooling capabilities of certain DSCs, we have considered the situation when the DSC instrument would not be able to perform certain fast cooling rates and the resulting q^- values would be lower than those programed. Set of simulated CHR cycles curves for $\Delta h^*/R = 45$ kK, $\ln(A/s) = 85$, $\beta = 0.6$, $x = 0.6$ was used as a base dataset. To imitate the distortion, the cooling rate $q^+ = 20$ °C min^{-1} was for the purpose of simulation lowered by 10 % (to 18 °C min^{-1}) and the cooling rate $q^+ = 50$ °C min^{-1} was lowered by 20 % (to 40 °C min^{-1}). In Fig. 13, the corresponding simulated DSC curves are shown. As can be seen, the distortion of the DSC curves appears to be very subtle. Nevertheless, even such very subtle distortion may lead to a significant shift of fictive temperature as shown in the inset in Fig. 13, where the evaluation according to Eq. 7 is shown. The corresponding increase of $\Delta h^*/R$ was ~ 2 kK.

Last type of data-distortion is associated with thermal lags arising due to the unideal heat conductivity of the samples. Similarly as in case of intrinsic cycle tests, we have assumed that it takes 3 extra seconds for the real sample to adopt the temperature of the furnace/pan and for the response signal to reach the sensor. Such thermal lag results in temperature shift of the DSC curve toward higher temperature—this effect naturally varies with applied heating rate. For the standard heating rate $q^+ = 10$ °C min^{-1}, the shift in all evaluated T_fs was +0.5 °C, which consequently lead to a decrease of determined $\Delta h^*/R$ by 0.1 kK for all tested combinations of TNM parameters.

Conclusions

Three most common methodologies for determination of activation energy of the glass transition phenomenon were analyzed in detail. The testing was performed for extensive amount of simulated data covering all types of structural relaxation behavior. Out of the three tested methodologies, it is the evaluation of Δh^* from intrinsic cycles that provide most accurate and reliable results. The evaluation based on a shift of T_p (according to Eq. 6) is very robust with respect to various kinds of data-distortive effects. The method is practically independent from the choice of temperature range for the cycles, as long as at least major part of the C_p change occurs during cooling. Distortions associated with

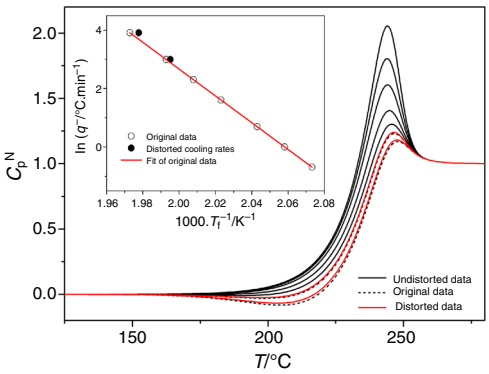

Fig. 13 Demonstration of data-distortive effect imitating inability of DSC instrument to perform very high cooling rates during CHR cycles; the data were simulated for $\Delta h^*/R = 45$ kK, $\ln(A/\mathrm{s}) = -85$, $\beta = 0.6$, $x = 0.6$, and $q^+ = 10$ °C min^{-1}. The inset then shows influence of such distortion on the evaluation of Δh^*

cooling and heating rates are easily identifiable from both the normalized C_p^N data and the $\ln(q^+) - T_p^{-1}$ dependence so that one can avoid involvement of the distorted data into the evaluation. In order to exploit the widest possible range of cooling and heating rates, the optimum q^+/q^- ratio would be $\approx$1.5–2 with the main limiting aspect being the insufficient heat conductivity of the sample in case of very high heating rates.

Considerably more prone to various data-distortive effects is the evaluation of Δh^* from CHR cycles. Namely the incorrect recognition of manifesting undershoot effects may have strong influence on accuracy of T_f determination and, consequently, on Δh^* evaluation. Bearing that in mind, great care needs to be taken during selection of proper temperature range for CHR cyclic experiments and during subtraction of the thermokinetic background (determination of the $C_{pg} - T$ and $C_{pl} - T$ dependencies). In this regard, it is extremely profitable to apply higher-than-standard heating rates during the CHR cycles. Faster heating scans not only result in more pronounced DSC signals (making the errors associated with inaccurate $C_{pg} - T$ and $C_{pl} - T$ extrapolations less significant) but also they effectively suppress the occurrence of the undershoot effects, which in consequence leads to easier and more accurate separation of the glass transition phenomenon from the thermokinetic background. Another argument for utilization of higher q^+ is that the thermal lag distortions have a negligible effect on Δh^* evaluation from CHR cycles.

Lastly, the curve-fitting procedure is most influenced by various data-distortive effects because precise thermal history as well as the overall shape of the DSC curve is taken into account during the non-linear regression. Thus curve-fitting is not recommended as a sole method for Δh^* determination. Consistency of the other evaluated TNM parameters (A, x, β) with respect to varying experimental conditions may imply high-quality measurements, correct acquisition of the data, and an accurate curve-fitting procedure.

Acknowledgements This work was supported by the Czech Science Foundation under project No. P106/11/1152.

References

1. Scherer GW. Relaxation in glass and composites. New York: Wiley; 1986.
2. Svoboda R, Málek J. Glass transition in polymers: (in)correct determination of activation energy. Polymer. 2013;54:1504–11.
3. Svoboda R, Čičmanec P, Málek J. Kissinger equation versus glass transition phenomenology. J Therm Anal Calorim. 2013;114:285–93.
4. Tool AQ. Relation between inelastic deformability and thermal expansion of glass in its annealing range. J Am Ceram Soc. 1946;29:240–53.
5. Narayanaswamy OS. A model of structural relaxation in glass. J Am Ceram Soc. 1971;54:491–7.
6. Moynihan CT, Easteal AJ, DeBolt MA, Tucker J. Dependence of the fictive temperature of glass on cooling rate. J Am Ceram Soc. 1976;59:12–6.
7. Hodge IM, Berens AR. Effects of annealing and prior history on enthalpy relaxation in glassy polymers. 2. Mathematical modeling. Macromolecules. 1982;15:762–70.
8. Svoboda R, Málek J. Description of macroscopic relaxation dynamics in glasses. J. Non-cryst Sol. 2013;378:186–95.
9. Hutchinson JM, Kovacs AJ. Effects of thermal history on structural recovery of glasses during isobaric heating. Polym Eng Sci. 1984;24:1087–103.
10. Hutchinson JM, Ruddy M. Thermal cycling of glasses 2 experimental evaluation of the structure (or non-linearity) parameter x. J Polym Sci B. 1988;26:2341–66.
11. Hutchinson JM, Ruddy M. Thermal cycling of glasses, III upper peaks. J Polym Sci B. 1990;28:2127–63.
12. DeBolt MA, Easteal AJ, Macedo PB, Moynihan CT. Analysis of structural relaxation in glass using rate heating data. J Am Ceram Soc. 1976;59:16–21.